Structure-Property analysis of in-situ Al-$MgAl_2O_4$ Metal Matrix Composites synthesized using ultrasonic cavitation

V.M. Sreekumar[1*], N. Hari Babu[1], D.G. Eskin[1], Z. Fan[1]
[1]BCAST, Brunel University, UB8 3PH, United Kingdom
*Email:Sreekumar.VadakkeMadam@brunel.ac.uk

Abstract

In-situ Al-$MgAl_2O_4$ metal matrix composite was successfully manufactured using SiO_2 with the aid of ultrasonication. $MgAl_2O_4$ particles and their clusters were identified at grain boundaries and interdendritic regions within the grain envelopes. The composite showed 2-5 fold of grain size reduction with respect to the reference alloy cast at similar conditions. The composite has shown 10% increase in yield stress and 15% increase in UTS while maintaining the ductility similar to reference alloy. CTE mismatch strengthening and grain boundary strengthening are suggested to be influencing in the improvement in mechanical properties.

1. Introduction

Metal–matrix composites (MMCs) have been extensively studied in the last few decades because of its demanding applications in aerospace, automobile, and military industries, etc. However, MMCs tend to fracture easily due to their poor ductility and low fracture toughness hindering their widespread use [1]. In recent times, research has been focused on MMCs reinforced with submicron and nano ceramic particles (MMNCs) [2, 3]. These MMCs are believed to overcome the disadvantages associated with the conventional MMCs. Also properties of conventional MMCs can be enhanced considerably even with a much lower volume fraction of these fine particles. In order to achieve better mechanical properties in MMCs especially prepared through casting process, it is necessary that ceramic particles are homogeneously distributed in molten metal. However, clustering of particles and poor wettability in liquid metal often prevent in achieving required casting quality [4]. More often, mechanical stirring using an impeller is not adequate to improve the dispersion of particles. While particles larger than 20-50 μm are successfully dispersed using impeller mixing alone, fine (sub-microns to a few microns) particles containing MMCs tend to form larger clusters. Recently ultrasonic cavitation and high shearing techniques are found to be helpful in the de-agglomeration and dispersion of fine and nano particles in Al and Mg alloys [5,6]. In order to tackle the wettability issue, several works have already been conducted on in-situ MMCs where fine ceramic particles are generated inside molten Al by chemical reactions. The in-situ MMCs such as Al-AlN, Al-TiC, Al-TiB_2 composites have shown better properties compared to conventional MMCs [7-9]. In-situ particles

of TiB_2, TiC, Al_2O_3, $MgAl_2O_4$ have demonstrated close crystallographic matching with Al that possibly negates the influence of macro scale wettability issue with Al [10,11]. Recently, Al_2O_3 and $MgAl_2O_4$ have got more attention due to their natural formation tendency on the Al alloy surface at different experimental conditions [11]. Also they are formed as interfacial products on any solid oxygen source (i.e., oxides) inside the molten Al [12]. The oxides such as SiO_2, TiO_2, B_2O_3 were found to be prone for reaction with Al at any experimental condition [13-15]. A few studies were made on the possibility of converting these oxides into in-situ Al_2O_3 or $MgAl_2O_4$ particles in an Al alloy [14, 15]. However, complete reaction of parent oxide and dispersion of these in-situ particles in Al are yet to be achieved.

In this paper, research is being directed to the synthesis of an MMC containing in-situ $MgAl_2O_4$ (spinel) particles using SiO_2 and ultrasonication technique. The paper details the reaction and dispersion of in-situ $MgAl_2O_4$ in Al. The microstructure and mechanical properties of the composite are investigated. Also the paper looks onto the possible reason behind the improvement of the properties as compared to a reference alloy.

2. Materials and Methods

Commercially pure Al (0.08wt%Si-0.1wt%Fe-remaining Al) and commercially pure Mg (99.97wt%) were taken as initial metals. SiO_2 was chosen as a solid oxygen source for $MgAl_2O_4$ formation. The particle size of the oxide supplied by Sigma-Aldrich was varied from 0.5 to 10 μm (more than 80% between 1 and 5 μm). Initially, 2 wt% of Mg wrapped in Al foil was diluted in 2.5 kg of superheated Al at 750 ^{0}C with minimum loss. 3 wt% of SiO_2 particles was stirred in the molten Al-Mg alloy at temperature between 650 and 700 ^{0}C using a mechanical impeller made up of a Ti alloy. The impeller was coated with high temperature ceramic material to minimize Ti pickup in Al melt during processing. The stirred metal was heated up and held at 900 ^{0}C for 30 mins to facilitate the reaction between SiO_2 particles and Al. Later, the molten metal was mixed with the impeller and simultaneously ultrasonicated (17.5 kHz, 3.5 kW, 40 micron amplitude, Nb sonotrode) for 5 min at 680-710 ^{0}C to ensure the dispersion of $MgAl_2O_4$ particles and complete the reaction of silica particles. The holding and mixing processes were repeated three times and the composite was cast at 725 ^{0}C in a steel wedge mould (Figure 1) [16]. The mould was preheated at 200 ^{0}C and metal was cast using a bottom pouring arrangement to ensure minimum porosity in the casting. The matrix alloy composition of the composite was analysed using Optical Emission Spectroscopy (Foundry Master Pro, Oxford Instruments). For comparison, a matrix alloy with similar composition was prepared by melting commercially pure Al, Al-20wt%Si master alloy and Mg, and treated for 5min with ultrasonication. The casting was done in the same wedge mould under similar casting conditions.

The samples for mechanical and microstructural studies were taken from different sections of the casting (top, bottom, R1/C1, R2/C2, R3/C3, R4/C4, R5/C5) shown in Figure 1. Five tensile samples were prepared from the sections mentioned in the diagram (R1/C1, R2/C2, R3/C3, R4/C4, R5/C5,) using ASTM standard (B557-06) for both reference alloy and composite. 'R' and 'C' respectively denote reference and composite samples (Figure 2). The tensile test was carried out in Instron 5569 with 50 kN load cell. All samples were used for microstructural and grain refinement analysis. For grain refinement studies, polished samples were anodized using 0.5% HBF_4 solution for approximately 1 min at 20 V and analysed in polarized light. For microstructural studies, Optical microscopy (Zeiss Axioscope), SEM (Zeiss Supra 35VP) and EDX (EDAX) were used. Phase identification in the composite was carried out using X-Ray Diffraction (Bruker D8 Advance). Micro hardness of the composites and reference alloy was measured using Wilson Hardness 432SVD.

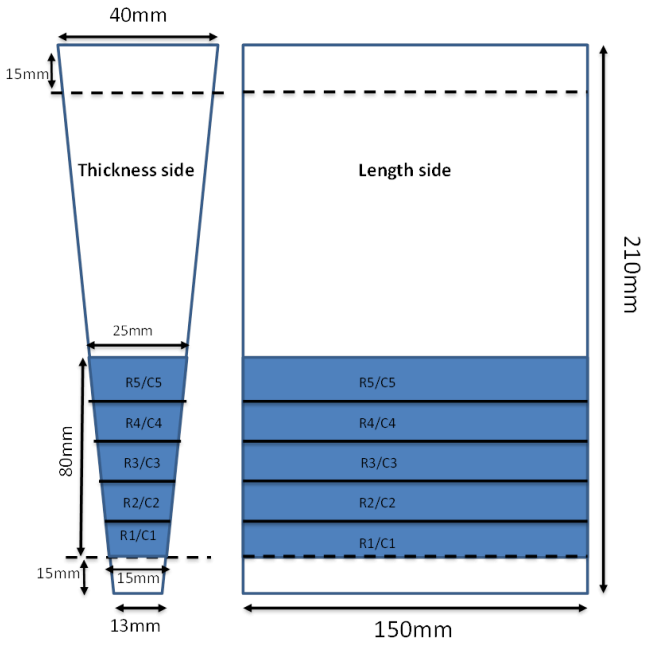

Figure 1. Diagram of casting with dimensions (not in scale). C1-C5 and R1-R5 denote the position of samples taken for tensile test.

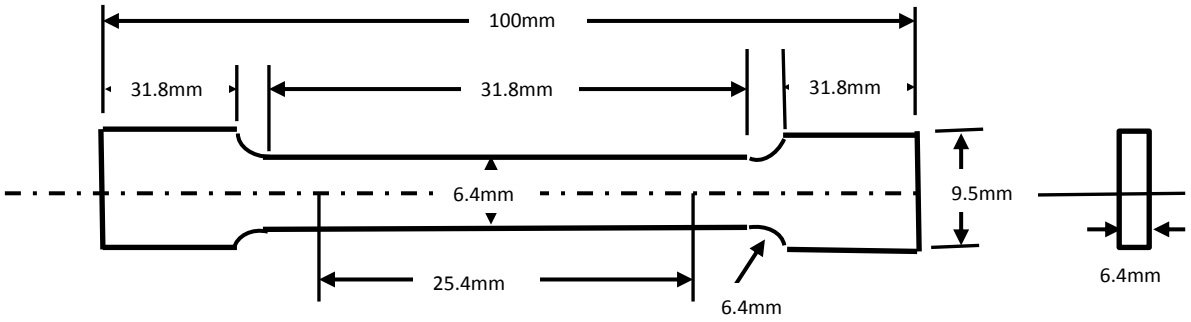

Figure 2. Diagram of Tensile specimen (ASTM B557-06) (not in scale)

3. Results and Discussion

Table 1. Composition of Al-$MgAl_2O_4$ composite and reference alloy

Material	**Mg**	**Si**	**Fe**	**Ti**
Al-$MgAl_2O_4$ composite (matrix composition)	1.34±0.03	1.5±0.05	0.1±0.03	0.015±0.003
Reference alloy	1.33±0.03	1.4±0.05	0.1±0.03	0.009±0.003

Table 1 details the matrix composition of composite and reference alloy. The reference alloy and matrix of the composite showed similar of Si, Mg and Fe compositions. 1.5 wt% of Si present in the composite was likely to come from the reaction between SiO_2 and molten Al alloy during the experiment. It was calculated from the displacement reaction (2) (describes later) that, 3wt% of SiO_2 forms ~3.5 wt% of $MgAl_2O_4$ and releases ~1.5 wt% Si into the matrix. Completion of reaction can be confirmed from the Si composition of the composite given in the table. Also, 1.3wt% Mg was found to remain in the alloy after the reaction and oxidation (burning) at higher temperatures. Ti composition of the composite was found to increase by ~0.01wt% probably from the impeller during experiment.

3.1. Microstructure of Al-$MgAl_2O_4$ composite

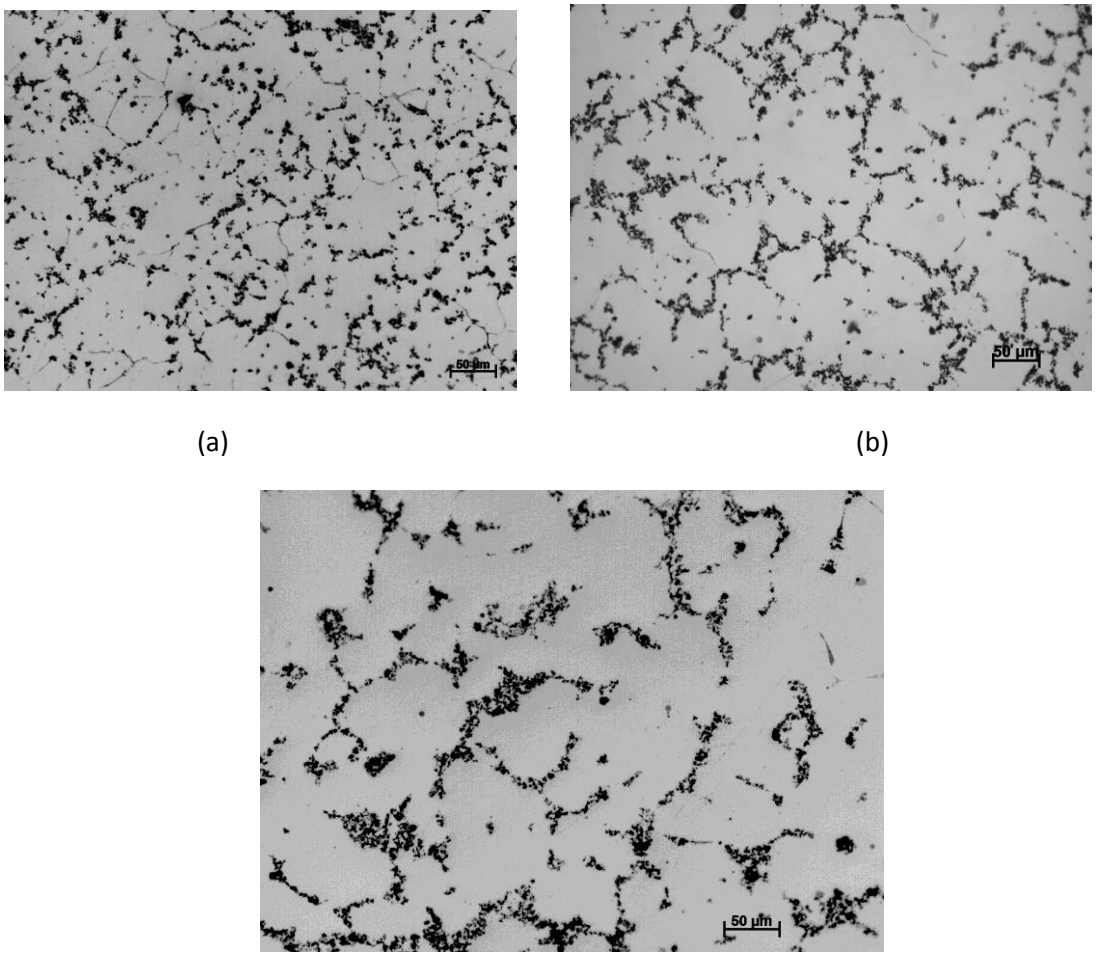

(a) (b)

(c)

Figure 3. Microstructure of Al-$MgAl_2O_4$ composite taken from (a) bottom of the casting (b) tensile test sample C5 (c) top of the casting

Figure 3 shows the microstructure of Al-$MgAl_2O_4$ composite taken from different sections of the casting. The particles (dark spots) were found to disperse along the grain boundaries or the dendritic arm boundaries within the matrix. Hereafter, grain boundaries and dendritic boundaries will be called as boundaries in the paper. The width of dendrite arms or α-Al was found to be increased from bottom (Figure 3(a)) to top of the casting (Fig 3(c)), which reflects the difference in cooling rate in the casting along the height. The change in the dendritic arm spacing will be discussed more in next section. Fine clusters of particles were observed at the bottom of the casting, whereas size of clusters was found larger on the top of the casting. $MgAl_2O_4$ particles were present together with the Mg_2Si phase from the microstructures.

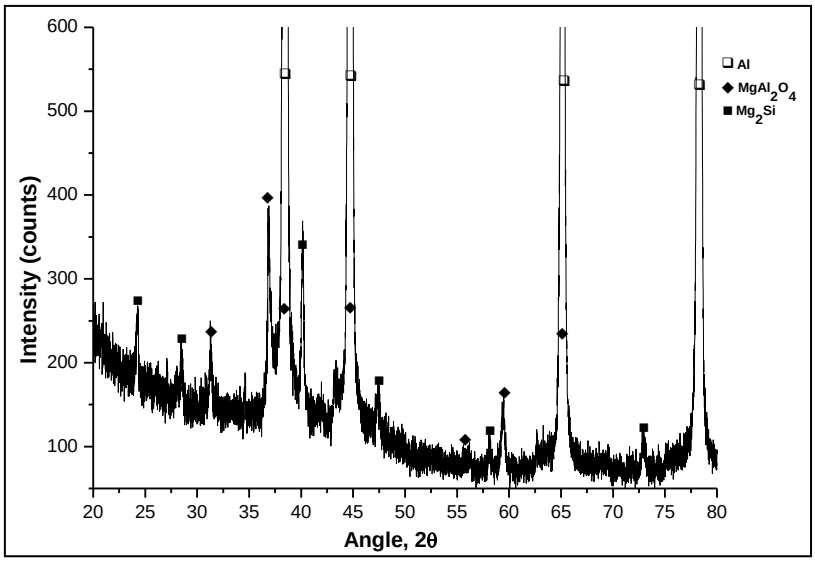

Figure 4. X-ray diffraction of Al-$MgAl_2O_4$ composite

$MgAl_2O_4$ and Mg_2Si phases were identified from the XRD analysis of the composite (Figure 4). The large peaks of $MgAl_2O_4$ phases represent their prominent presence in the composite.

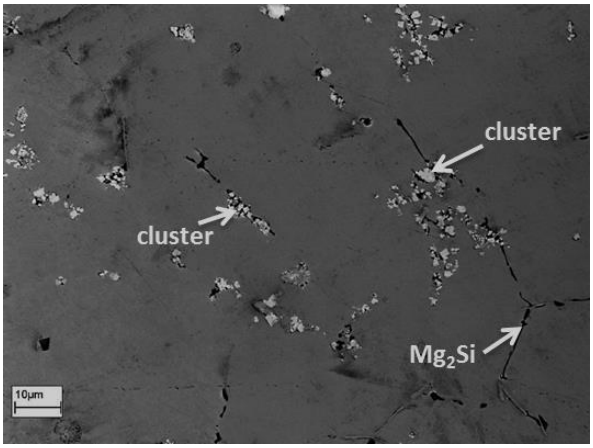

(a)

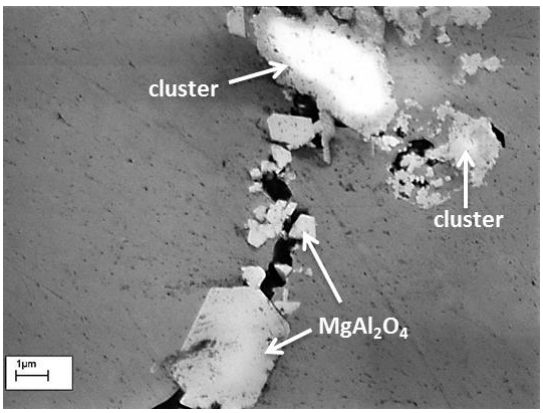

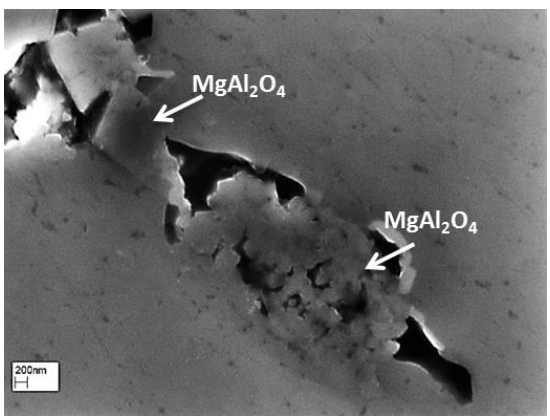

(b) (c)

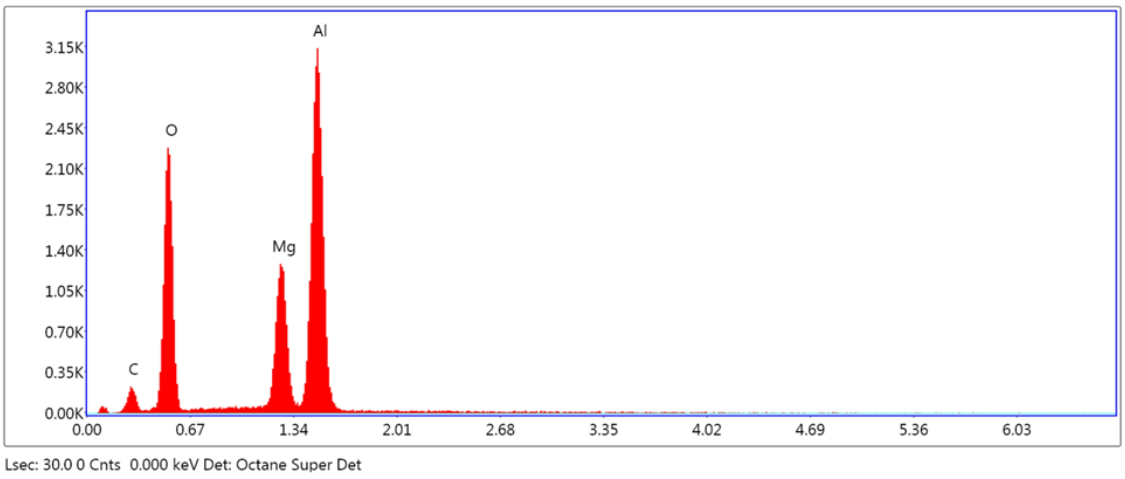

(d)

Figure 5. (a), (b) and (c) SEM images of Al-$MgAl_2O_4$ composite (bottom of the casting) (d) EDS of $MgAl_2O_4$ particle

The SEM image (Figure (5a)) shows several $MgAl_2O_4$ clusters (white spots) along with Mg_2Si in the matrix (Figure (5(a)). The particle clusters were identified to be similar in the size to SiO_2 particles (~5-6 µm) (Figure 5(b)). These clusters would have formed during the growth of crystals or the solidification process. The size of $MgAl_2O_4$ particles (crystal) was varied from 200 nm to 2 µm in different places (Figure 5(c)), Smaller particles are found as clusters whereas larger sized particles were separated in the matrix. Larger $MgAl_2O_4$ particles with ~10 µm were also found but rarely in the microstructures (Figure 5(b)). All these suggest a random crystal growth at the experimental conditions. The presence of $MgAl_2O_4$ was further confirmed by EDS (Figure (5(d)), where the Mg, Al, O phases were identified on the crystals found along the boundaries (Figure 5(c)). Formation and dispersion of $MgAl_2O_4$ crystals in Al is discussed in the following section.

3.1.1. Formation, growth and dispersion of $MgAl_2O_4$ crystals

Important displacement reactions between SiO_2 and an Al-Mg alloy at 750^{0}C are given below [17]. Because the standard Gibbs free energy is negative for all the reactions at the processing temperatures (650-900 ^{0}C), the formation of Al_2O_3, $MgAl_2O_4$, and MgO phases is thermodynamically feasible.

$$SiO_{2(s)} + 2Mg_{(l)} \rightarrow 2MgO_{(s)} + Si_{(l)},\ \Delta G^0 = -268.22\ kJ\ mol^{-1} \quad (1)$$

$$2SiO_{2(s)} + Mg_{(l)} + 2Al_{(l)} \rightarrow MgAl_2O_{4(s)} + 2Si_{(l)},\ \Delta G^0 = -449.632\ kJ\ mol^{-1} \quad (2)$$

$$3SiO_{2(s)} + 4Al_{(l)} \rightarrow 2Al_2O_{3(s)} + 3Si_{(l)},\ \Delta G^0 = -556.44\ kJ\ mol^{-1} \quad (3)$$

$3SiO_{2(s)} + 2MgO_{(s)} + 4Al_{(l)} \rightarrow 2MgAl_2O_{4(s)} + 3Si_{(l)}$, $\Delta G^0 = -631.084$ kJ mol^{-1} (4)

The Al_2O_3-$MgAl_2O_4$-MgO phase equilibria existing in oxide-reinforced Al-MMCs was studied by thermodynamic models and experimentally verified with different Mg composition of matrix alloy elsewhere [18]. The studies established that Al_2O_3 forms at very low Mg content (<0.19 wt%), whereas $MgAl_2O_4$ is stable between 0.007 and 10 wt% Mg and MgO is stable at >7 wt% Mg. Hence, only $MgAl_2O_4$ can be stable in Al-2 wt% Mg-3 wt% SiO_2 used in the present study, which is confirmed by XRD analysis. Apart from thermodynamic stability, kinetics factors such as temperature and time contribute onto the formation, growth and clustering of reaction products on the parent oxides particles. Disintegration of clusters completes the reaction of oxide particles. So, the dispersion of $MgAl_2O_4$ in Al alloy may follow the events schematically shown in Figure 6.

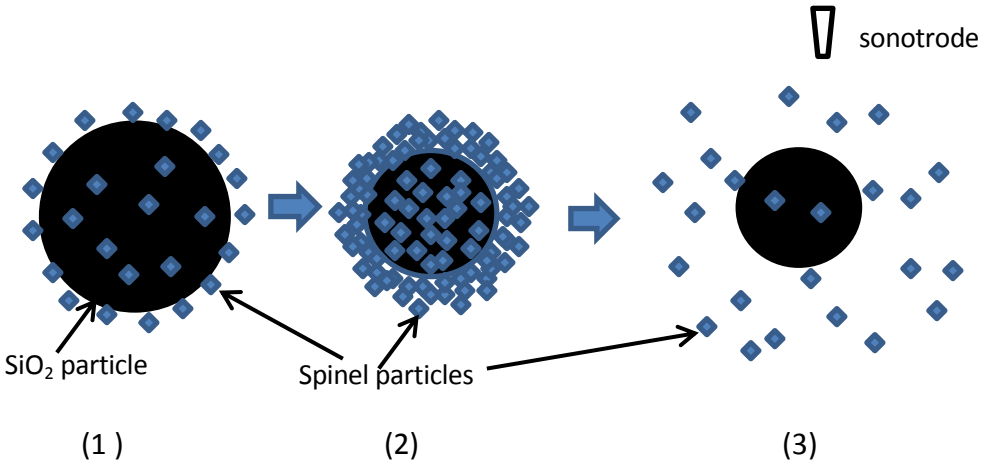

Figure 6: Schematic of spinel dispersion in Al (1) Reaction of oxides (2) clustering of spinel (3) Disintegration of clusters.

In Al-2 wt% Mg-3 wt% SiO_2 system, reactive wetting is observed through the reaction product such as $MgAl_2O_4$ crystals formed by displacement reactions (2) and (4) at the particle–liquid interface. Interfacial energy is reduced by the chemical reactions between Al, Mg and SiO_2 and the formation of $MgAl_2O_4$ at the liquid Al-SiO_2 interface (event 1) in Figure 6 [19]. Once surface reaction is initiated, Si atoms start diffusing into the surrounding molten metal. The reaction propagates towards the interior of the particle along with the surface reaction. After the formation of the first layer of $MgAl_2O_4$; Mg, Al, and the released Si must diffuse through the reaction layer to enable reactions at the interior of the particles. The formation of $MgAl_2O_4$ from SiO_2 will result in a 27% volume contraction [20]. Owing to this contraction, gaps are formed between the newly formed crystals or between the newly formed crystals and the rest of SiO_2.

Liquid Al and Mg infiltrate into these gaps and form so called 'diffusion channels' [20]. The surface reaction and wetting are continued till the particle surface is completely reacted. Further, the bulk reaction of the particles has been found to cease with the time as the product crystals become accumulated on the path of the diffusion channels. This will eventually results clustering of reaction products having 200-500 nm size crystals bonded by Van der waals force and yet to be separated from the parent SiO_2 particles (event 2). The above reaction mechanism is very similar to template growth of $MgAl_2O_4$ crystals on the parent crystals of Al_2O_3 during molten salt synthesis [21]. Disintegration of clusters is a necessary event to disperse the $MgAl_2O_4$ crystals in the alloy and ultrasonic cavitation was found helping in the dispersion process.

Introducing the ultrasonic waves in the melt causes acoustic cavitation and streaming effects. Acoustic cavitation occurs through the formation, growth and collapse of cavitation bubbles under alternate acoustic pressure wave cycles [5]. Molten Al always contains dissolved gases. Above the cavitation threshold, entrapped gas generates numerous tiny cavities. Upon pulsation, these cavitation bubbles grow by rectified diffusion of gases from the melt [22]. Cavitation bubbles of a particular size implodes during positive pressure cycle generating a temperature of ~5000 ^{o}C and pressure of ~1000 MPa and forms a liquid jet of ~100 m/s in the vicinity of cavitation implosion region [23]. Simultaneously, acoustic streaming of 0.1m/s formed from the pulsation of the cavitation region ensures continuous stirring effect throughout the melt [24]. During ultrasonication, cavitation and acoustic streaming are believed to improve the wettability of parent oxides and enhance the displacement reactions. Also, cavitation pressure and the liquid jet created by the implosion of the bubbles can disintegrate the reaction product agglomerations from the interface leaving new surface for reaction (event 3). Another possibility is that pressure created by cavitation implosion is sufficient to disintegrate large SiO_2 particles. These can dramatically change the kinetics of the reactions. Further, cavitation and acoustic streaming can prevent any formation of large clusters within the liquid metal. Previously, the first author noticed partial reaction of SiO_2 (~55%) in Al-5 wt% Mg-5 wt% SiO_2 composite even after impeller mixing and holding of the metal for 10 hrs at 750-900 ^{0}C [17, 25]. Partially reacted silica (SiO_2) particles were found as agglomerates in the matrix (Figure 7(a) and the $MgAl_2O_4$ particle clusters were found on SiO_2 surface (Figure 7 (b) [25]. In the present study, the micro-meter and nano-meter sized $MgAl_2O_4$ crystals distributed within the matrix leaves an impression that application of ultrasonication is beneficial in completing the reaction and dispersion of $MgAl_2O_4$ crystals.

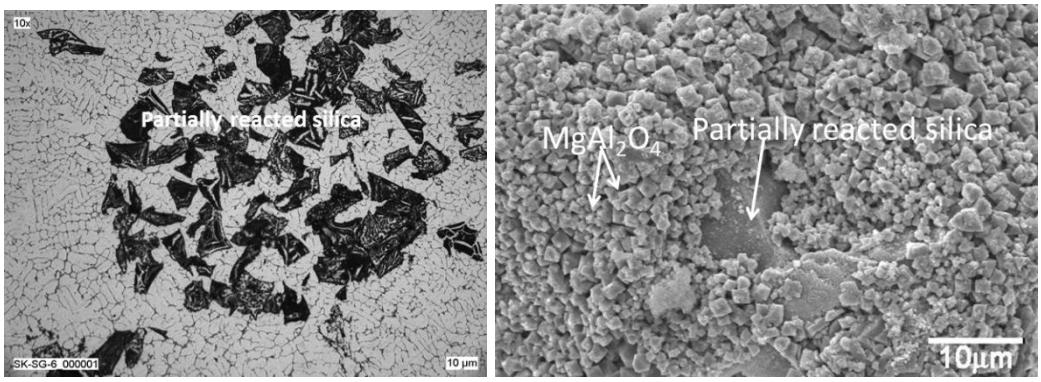

(a) (b)

Figure 7: Al-5 wt% Mg-5 wt% SiO_2 composite mixed and held for 10 hrs (a) Optical micrograph of the composite (b) SEM of partially reacted silica particle [25]

3.2.Grain refinement in Al-$MgAl_2O_4$ Composite

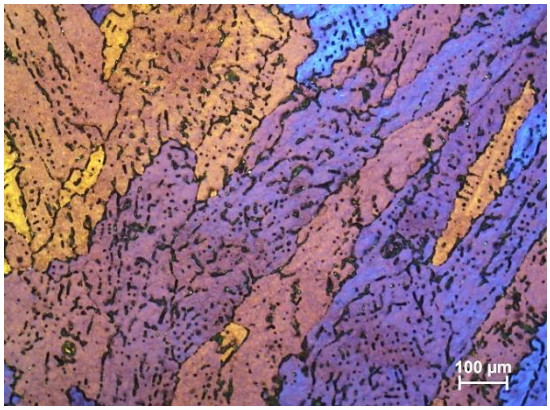

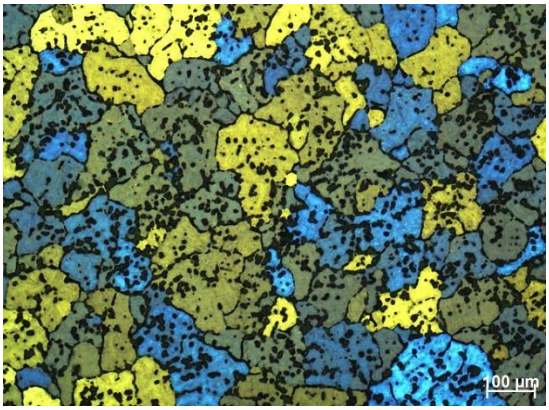

(a) (b)

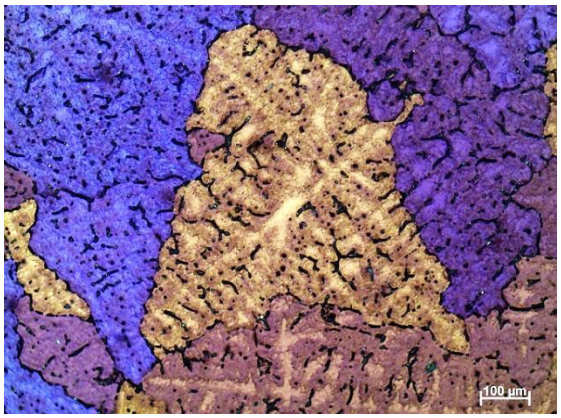

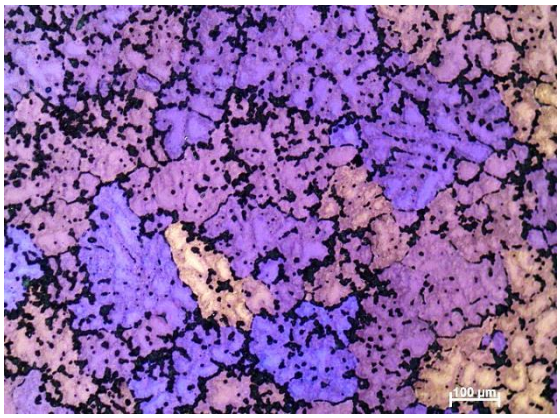

(c) (d)

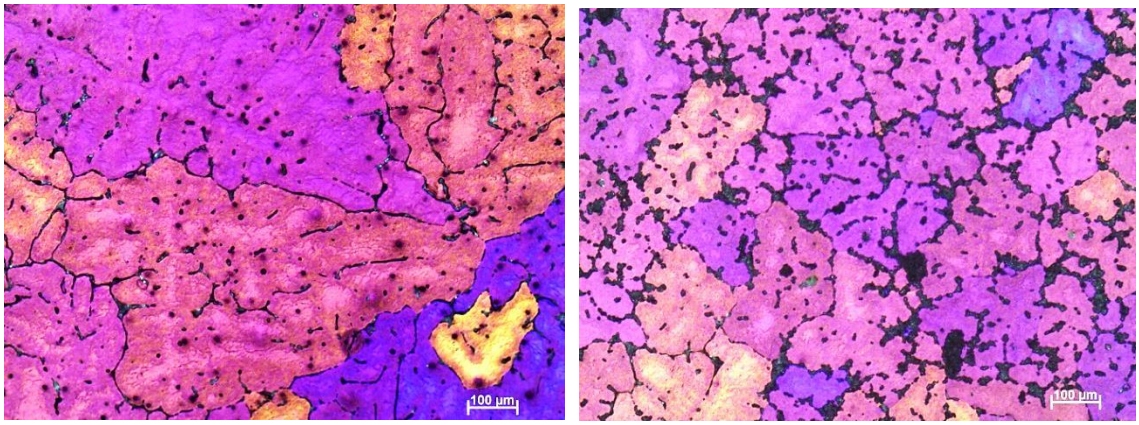

(e) (f)

Figure 8: Microstructure of anodized samples from different section of the casting (a) bottom (reference), (b) bottom (Al-$MgAl_2O_4$), (c) R1, (d) C1, (e) R5, (f) C5

Figure 8 shows the microstructures of anodized alloy and composite samples from bottom, R1/C1 and R5/C5 positions. It is clear that both alloy and composite went through dendritic solidification. Large columnar grains are present at the bottom of the casting for the reference alloy, whereas the equiaxed dendritic structure for composite. A clear reduction of grain size was observed in composite compared to reference alloy. It can be further confirmed from the figures that particles were distributed in the interdendritic regions as well as intergranular regions in composite. Figure 9 details the grain size and dendrite arm spacing distribution in composite and reference alloy along the height of the casting.

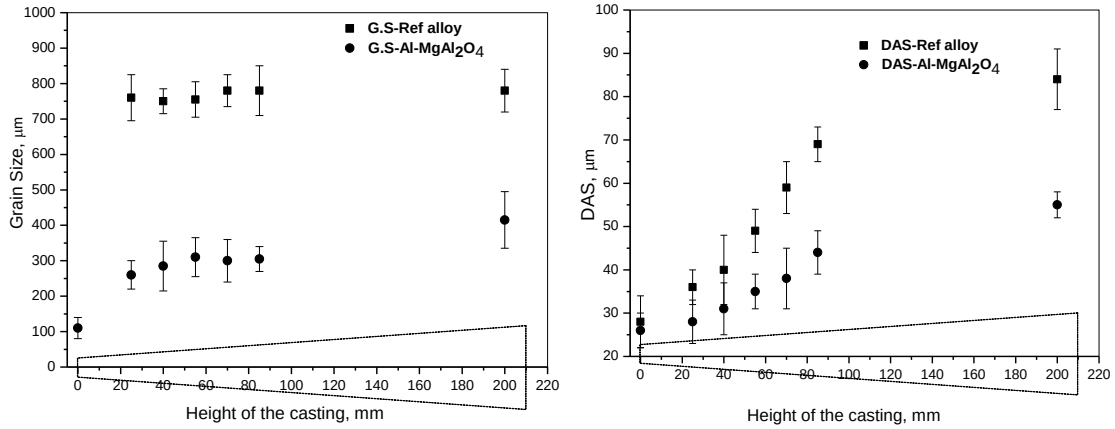

(a) (b)

Figure 9: (a) Grain Size (GS) and (b) Dendritic Arm Spacing (DAS) distribution in the reference alloy and composite along the height of casting

The grain size was found to be minimum at the bottom tip of the casting for the composite. Once going from the bottom to top of the casting, grain size was found to

be increased from 110 µm to 400 µm in the composite casting. However there was no obvious change in the grain size observed for reference alloy. All tensile samples of reference alloy and composite registered to be similar grain size (~800 µm for the reference alloy and ~300 µm for the composite) even though there was a small increase in the grain size (25-50 µm) observed from R1 to R5 and C1 to C5. In the present casting condition, the bottom part of the mould registered the highest cooling rate, where the finest grains were present in the case of the composite. The presence of columnar grains in the case of the reference ally denotes the absence of heterogeneous nucleants. There was a steady increase in the dendritic arm spacing from bottom to top of the casting for both the reference alloy and the composites. Smaller DAS was observed for the composite and the increase of DAS is slower than in the reference alloy. The increase in the DAS denotes a decrease in cooling rate from bottom to top of the casting. It is well understood that cooling rate has larger effect on DAS than on its grain size during the solidification of grain refined Al alloys [26]. Also noted from the analysis that average DAS of larger grains are finer than that of finer grain as in accounts for higher order branches present in larger grains. The grain refinement present in the Al-$MgAl_2O_4$ composite can be understood by its solidification history and nucleation potency of $MgAl_2O_4$ in Al.

3.2.1. Solidification of Al-$MgAl_2O_4$ composite

During the solidification of the composite containing individual $MgAl_2O_4$ particles or their clusters, the particles may be pushed or entrapped depending on their size or critical velocity of solidification front. From different particle pushing/engulfment theories, larger particles (10's to 100's of microns) are entrapped within the grain boundaries, which suggest thermal conductivity effect that blunts the solidification front [27]. In the case of smaller particles (clusters) (few hundred nano meters to a few microns), the predictions and experimental results suggest the particle motion as stokesian and solidification front is likely to push or entrap particles between secondary dendrite arms [27,28]. Youssef et al [16] conducted detailed study on particle pushing and engulfment in Al-TiB_2 composites (from 0.12 to 3.5vol%TiB_2) using similar casting (steel wedge mould of same dimensions) and solidification conditions, where TiB_2 particles were identified as clusters of 10-20 µm and pushed towards grain boundaries in all solidification velocities for CPAl-TiB_2 composites and A514-TiB_2 composites. Further, particle engulfment was present only at larger solidification velocities. So from the present casting conditions, it was likely that particles or their clusters were pushed by the growing dendrites in the beginning of solidification and entrapped within inter-dendritic regions during eutectic solidification. This is substantiated from the microstructures of Al-$MgAl_2O_4$ composite taken from bottom and top of the casting, where cooling rates and solidification velocities are different (Figure 10). The grains have equi-axed dendritic morphology and particles or clusters

were found inside the grain envelope and boundaries. The particle pushed towards grain boundaries act as barriers to grain growth resulting grain refinement in the final microstructure. There are several individual particles present within the grain envelope. The grain refinement and change in the grain morphology suggest that $MgAl_2O_4$ particles may act as heterogeneous nucleants as well.

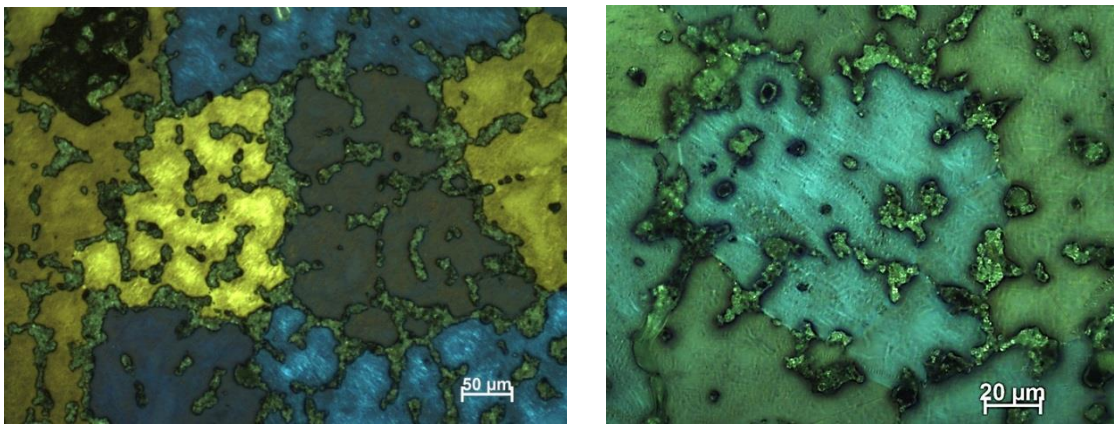

(a) (b)

Figure 10. Microstructure of Al-$MgAl_2O_4$ composite taken from (a) 10mm from the top of the casting (b) 10mm from the bottom of the casting

3.2.2. Nucleation potency and efficiency of $MgAl_2O_4$

There are a few theoretical studies and experimental data showing the potential of Al_2O_3 or $MgAl_2O_4$ as heterogeneous nucleants in Al. Recently, Atamanenko et al. [29] investigated the grain refining effect of exogenous oxides such as Al_2O_3 combined with ultrasonic treatment in pure Al (99.95% Al), and attributed the grain refinement to cavitation-induced heterogeneous nucleation through the activation of oxides. In addition, it was proposed that naturally occurring oxides such as MgO and $MgAl_2O_4$ in liquid Mg and Al alloys may respectively enhance heterogeneous nucleation in Mg and Al alloys treated with intensive melt shearing [11].

The interfacial free energy at the nucleating interface is one of the controlling factors in heterogeneous nucleation. The importance of low interfacial energy for a potent substrate has been demonstrated long ago by the classical nucleation theory. However, the issues related to perfect wetting of exogenous inoculants with molten Al often fail to reduce the interfacial energy to a lower level. Once particles are wetted as often found in in-situ composites, nucleating potency can be related to the lattice matching at the solid/substrate interface during heterogeneous nucleation. Better the lattice matching, higher the nucleation potency. In the present study, $MgAl_2O_4$ spinel was formed in-situ in molten Al. From cube on cube parallel orientation relation (OR) [30], to a mismatch of 2.5^0 along the [110] direction on the (111) plane was reported between Al and $MgAl_2O_4$ [31]. Also, the lattice misfit between $MgAl_2O_4$ and Al (1.4%)

was found to be smaller than that for the Al/TiB_2 system (-4.2%) [11]. All these satisfy the conditions for a potent substrate in the case of $MgAl_2O_4$. Nucleation efficiency refers to the effectiveness of a given type of inoculant with specific physical characteristics and solidification conditions, such as number density, size, size distribution, and cooling rate. The TiB_2 particle population in Al-5 wt% Ti-1 wt% B master alloy was estimated to be 10^8 particles/cc [32]. Similarly, for the size of $MgAl_2O_4$ crystals between 200 nm and 2 µm, $MgAl_2O_4$ particles in the composite was approximated to be between 10^{11} and 10^{14} particles/cc. The undercooling required for heterogeneous nucleation was calculated to be to be quite small for large particles of TiB_2 in Al-5 wt% Ti-1 wt% B master alloy (i.e, 1K for 500nm and 0.2K for 3 µm) [32], which may be true for $MgAl_2O_4$ crystals as well. In the present scenario, wetting was already established by reaction (ie., reactive wetting) and cavitation and associated acoustic streaming were found assist in the distribution of the particles throughout the metal ensuring more particles for the nucleation event.

It is interesting to look at the MMC systems such as A514-TiB_2 [16], AZ91-SiC [33] where particles play dual roles in achieving finer grains via heterogeneous nucleation and grain growth restriction. Ferguson et al proposed an empirical relation to predict the grain size of MMC at different volume percentage (V) of the particles as follows [34]:

$$D = D_0(1 + pV)^{-1/3} \quad (5)$$

where D and D_0 are the average grain size of the MMC and unreinforced alloy respectively. p is defined as refining power of the reinforcement for the alloy. Eventhough the relation considered grain growth restriction as the dominant mechanism, which is true for nano MMCs, it was well fitted for other Mg and Al MMCs containing different volume fraction of micron sized particles. Using this equation, the refining power of $MgAl_2O_4$ in the present study (Al-$MgAl_2O_4$) was calculated as 6.7 for D_0=800 µm and D=300 µm. The volume percentage (V) was calculated using the equation (6) as 2.7 which is equal to 3.5 wt%. d_p and d_m are the densities of $MgAl_2O_4$ (3.6 g/cc) [25] and Al (2.7 g/cc) respectively.

$$V = \frac{\frac{wt\%}{d_p}}{\frac{wt\%}{d_p} + \frac{100 - wt\%}{d_m}} \times 100 \quad (6)$$

The grain size of MMCs with respect to different volume fraction of particles is plotted in Figure 11. In a previous study by the first author, grain refinement was observed in

an A357 alloy at a very low volume fraction of in-situ $MgAl_2O_4$ particles [35]. The p value of $MgAl_2O_4$ in the A357 alloy system is calculated as 80 from Eq. 5. The 'D's for Al-$MgAl_2O_4$ and A357-$MgAl_2O_4$ systems with different $MgAl_2O_4$ content are extrapolated and plotted in Figure 11. It is demonstrated from the graph that particles at low volume percent give sharp reduction of grain size which may be due to dominant heterogeneous nucleation (presented with dotted circle). A subsequent reduction in the grain refinement effect at a higher volume of particles suggests a prevalent grain growth restriction mechanism as the number of heterogeneous nucleants may be fixed for any volume of particles. Needless to say that alloy composition plays an important role in grain refinement.

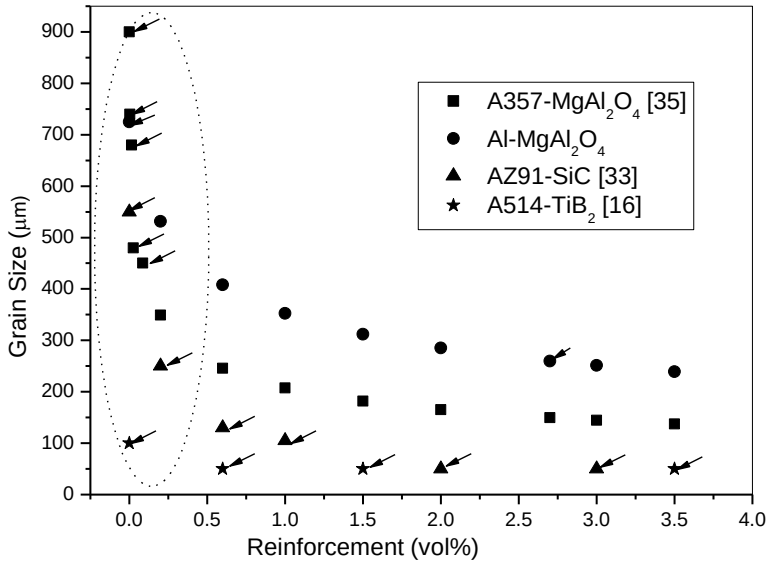

Figure 11. Plot between volume percentage of reinforcements and grain size for different composite/alloy systems. Arrows denote experimental results

Ti has influence on grain refinement and morphology change by its strong segregating nature (very high growth restriction factor, Q) [36]. It is well known that the grain size reduction by Ti addition is prominent in pure Al [36]. But in commercial alloys especially Si and Mg containing alloys, low Ti addition is not effective [37]. Thus, it is strongly believed that Ti pickup during composite preparation (~0.01wt%) has minimum influence on the solidification and the grain refinement present in the composite is the result of heterogeneous nucleation and grain growth restriction by $MgAl_2O_4$ particles.

3.3. Mechanical properties of Al- $MgAl_2O_4$ Composite

Figure 12 shows the stress-strain curves of as-cast reference alloy and composite and their values are present in Table 2. An improvement in the proof stress and UTS for the

composites can be noticed from the figure and table. Also, the toughness (area under the stress-strain curve) of the composite was found to be improved compared to the corresponding reference alloy sample. The micro hardness of the alloy was also increased with particles content.

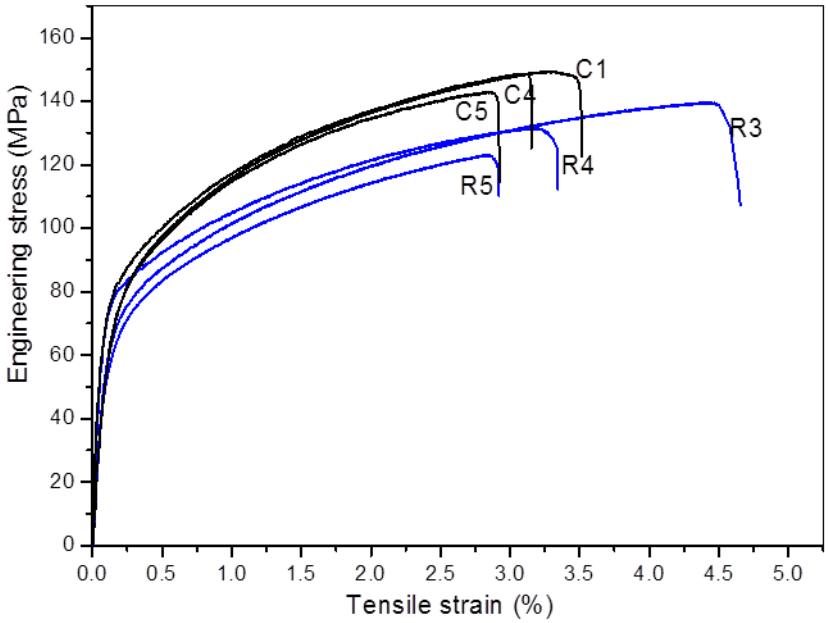

Figure 12. Engineering Stress-Strain graphs of Al-$MgAl_2O_4$ composites and reference alloy

Table 2. Comparison of mechanical properties of Al-$MgAl_2O_4$ composite and reference alloy

Material	Proof stress, MPa	UTS, MPa	Tensile strain (%)	Tensile Toughness, MPa x %	Microhardness (Hv 5kg)
Composite	87±2	147±4	3.1±0.3	C1=433, C4=389, C5=343	59±4
Reference Alloy	79±5	130±10	3.5±0.9	R3=531, R4=372, R5=293	49±3

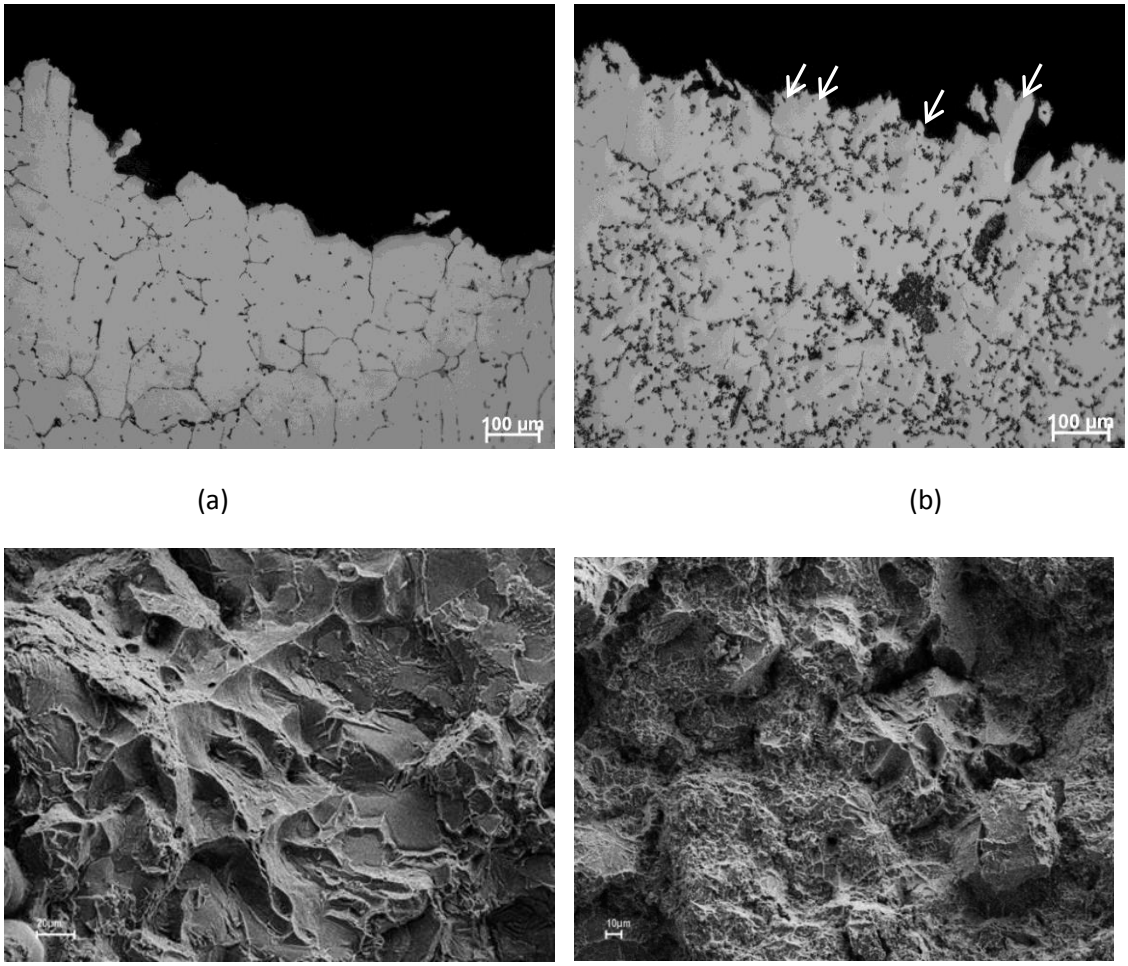

Figure 13. Optical and SEM micrographs of fracture surface of (a) and (c) reference alloy, (b) and (d) composite

The fracture surface of tensile tested alloy and composite is shown in optical and SEM micrographs (Figure 13). Large dimples were found on the surface of the alloy, whereas the size of simples was quite small in composites denoting a ductile fracture for both alloy and composites (Figure 13 (c) and (d)). Interdendritic or intergranular failure was observed in alloy (Figure 13(a)) and composite (Figure 13(b)) and clusters of $MgAl_2O_4$ particles were found along the fracture area of the composite (shown by arrows in Figure 13 (b)). A similar observation was made from the failure analysis of 6061 alloy reinforced with larger and finer SiC particles where initiation and propagation of crack in the ductile matrix were found to associate with individual particles in larger SiC particles reinforced composite, whereas boundaries between the particle clusters and surrounding matrix were found responsible for the failure of fine particle reinforced composites [38]. Further in well-bonded fine particle reinforced composites, the particles behave like precipitates where energy consumption for voiding, debonding or seperation between reinforcements and surrounding matrix

becomes larger while plastic deformation energy of the matrix remain same [38]. Similarly, a higher toughness observed in an Al-TiB_2 composite was believed to be due to homogeneous distribution of TiB_2 particles (clusters) [9]. The particle distribution may homogenize stress distribution and minimize the opportunity for multiple slip band piles [9].

3.4. Strengthening mechanisms

The improvement in stress and ductility by addition of particles may be governed by different strengthening mechanisms. The Al-$MgAl_2O_4$ MMC may exhibit strengthening mechanisms such as load bearing, grain boundary and coefficient of thermal expansion (CTE) mismatch. The influence of Orowan strengthening is considered to be insignificant in the present scenario since the $MgAl_2O_4$ crystals or their clusters were found as a few hundered nano meters to a few microns in size and were mostly located at the boundaries.

3.4.1. Load bearing strengthening

This strengthening mechanism explains the direct strengthening contribution from the presence of reinforced particles. In the case of well-bonded reinforcement particles to matrix,

$$\Delta\sigma_{Load} = 0.5V_p\sigma_m \quad (7)$$

where $\sigma_m$is the yield strength of matrix alloy (79 MPa) from the Table 2, V_p is the volume fraction of $MgAl_2O_4$ (0.027). σ_{Load} was calculated to be ~1 MPa, which demonstrates a negligible change in the strength due to load bearing of the reinforcement.

3.4.2.Grain refinement strengthening

There are empirical models available for predicting the yield stress change due to the change in grain size in MMCs by extending the Hall-Petch relationship as follows [39]:

$$\Delta\sigma_{GR} = k_y(D^{-1/2} - D_0^{-1/2}) \quad (8)$$

where D and D_0 are the average grain size of the composite (300 µm) and unreinforced alloy (800 micron) respectively. This equation assumes that Hall-Petch parameters K_y (~68 MPa $(\mu m)^{1/2}$ for Al alloys [40]) and σ_0 remain unchanged in the composites during processing. From the equation, $\Delta\sigma_{GR}$ was calculated as ~1.5 MPa. In dendritic alloys, the mechanical properties are also related to their DAS. So the average DAS of the reference alloy and composite was estimated to be 52 µm and 37 µm respectively from Figure 9 (b). By substituting these values to D_0 and D, $\Delta\sigma_{GR}$ was obtained as 1.7

MPa. Even though appreciable grain refinement was observed, the influence of grain refinement strengthening was estimated to be small. So it is worth looking onto the influence of CTE mismatch strengthening.

3.3.2.4. Coefficient of Thermal Expansion (CTE) mismatch strengthening

When MMC is quenched from processing temperature to room temperature, volumetric strain mismatch between matrix and reinforcement particles may occur due to difference in CTE, which subsequently produces geometrically necessary dislocations around reinforcement particles to accommodate the CTE difference. When the length of generated dislocation loop is assumed as πd_p, the strength increment from CTE strengthening can be estimated by [39]

$$\Delta\sigma_{CTE} = \beta G b (\rho^{CTE})^{1/2} \quad (9)$$

where β is a constant ~1.25.

and $G = 0.5E_m/(1+\vartheta)$ (10)

G is the shear modulus, E_m is the young modulus of matrix alloy, 68 GPa, ϑ is the Poisson's ratio, 0.33, b is the Burger's vector (0.286nm), ρ^{CTE} is the dislocation density induced by CTE mismatch, which can be calculated by the equation [35]

$$\rho^{CTE} = \frac{12(\alpha_m - \alpha_p)\Delta T V_p}{b d_p (1 - V_p)} \quad (11)$$

Where α_m is CTE of matrix (23 x10^{-6}/K) [9] and α_m is CTE of particle (8.1x10^{-6}/K) [41]. ΔT is the difference between processing temperature (725 ^{0}C) and room temperature (25 ^{0}C). d_p is taken as the average size of the clusters, (~6 µm). V_p is the volume fraction of particles (0.027). $\Delta\sigma_{CTE}$ is estimated as ~10 MPa. This showed that CTE mismatch can be a dominant strengthening mechanism in the present study.

Conclusions

1. Al-3.5$MgAl_2O_4$ in-situ composite was successfully manufactured using a solidification processing with the aid of ultrasonication. The homogeneous bulk distribution of $MgAl_2O_4$ particles and their clusters were identified in grain boundaries and interdendritic regions. Complete reaction of parent oxide (SiO_2) was achieved.
2. The composite showed 2-5 fold of grain size reduction with respect to the reference alloy cast at similar conditions.
3. The composite showed 10% increase in yield stress and 15% increase in UTS while maintaining the ductility similar to reference alloys. Interdendritic or intergranular fracture was observed in alloy and composite.

4. CTE mismatch strengthening and grain boundary strengthening were seemed to be influencing on the improvement of properties from the analysis.

Acknowledgement

The authors wish to acknowledge financial support from the ExoMet Project, which is co-funded by the European Commission in the 7th Framework Programme (contract FP7-NMP3-LA-2012-280421), by the European Space Agency and by the individual partner organisations.

References

1. D. J. Lloyd Aspects of fracture in particulate reinforced metal matrix composites. Acta Metall Mater 1991; 39(1):59-71.

2. J. Ye, B.Q. Han, J.M. Schoenung. Mechanical behaviour of an Al–matrix composite reinforced with nanocrystalline Al-coated B_4C particulates. Philos Mag Lett 2006; 86: 721–32.

3. B.F. Schultz, J.B. Ferguson, P.K. Rohatgi. Microstructure and hardness of Al_2O_3 nanoparticle reinforced Al–Mg composites fabricated by reactive wetting and stir mixing. Mater Sci Eng A 2011; 530: 87–97

4. D. R. Kongshaug, J. B. Ferguson, Benjamin F. Schultz, Pradeep K. Rohatgi Reactive stir mixing of Al–Mg/Al_2O_3np metal matrix nanocomposites: effects of Mg and reinforcement concentration and method of reinforcement incorporation. J Mater Sci 2014; 49: 2106–2116

5. G. I. Eskin, D. G. Eskin. Ultrasonic Treatment of Light Alloy Melts, Second Edition (Advances in Metallic Alloys). CRC Press, Boca Raton: 2014

6. N.S. Barekar, S. Tzamtzis, N. Hari Babu, Z. Fan, B.K. Dhindaw Processing of ultrafine-size particulate metal matrix composites by advanced shear technology. Metall. Mater. Trans. A 2009; 40(3): 691-701

7. Y.Q. Liu, H.T. Cong, W. Wang, C.H. Sun, H.M. Cheng AlN nanoparticle-reinforced nanocrystalline Al matrix composites: Fabrication and mechanical properties. Mater. Sci. Eng A 2009; 505: 151–156

8. X. C. Tong Fabrication of in situ TiC reinforced aluminium matrix composites Part I Microstructural characterization. J. Mater. Sci. 1998; 33: 5365 – 5374

4. J.B. Ferguson, F. S. Jaberi , C.S. Kim, P. K. Rohatgi , K. Cho On the strength and strain to failure in particle-reinforced magnesium metal-matrix nanocomposites (Mg MMNCs). Mater. Sci. Eng A 2012; 558: 193–204

9. Z. Chen, T. Wang, Y. Zheng,Y. Zhao, H. Kang, L. Gao Development of TiB_2 reinforced aluminium foundry alloy based in situ composites – Part I: An improved halide salt route to fabricate Al–5 wt%TiB_2 master composite Mater Sci Eng A 2014; 605: 301–309

10. M.X. Zhang, P.M. Kelly, M.A. Easton, J.A. Taylor Crystallographic study of grain refinement in aluminum alloys using the edge-to-edge matching model Acta Mater 2005; 53: 1427–1438

11. H.-T. Li , Y. Wang, Z. Fan Mechanisms of enhanced heterogeneous nucleation during solidification in binary Al–Mg alloys. Acta Mater. 2012; 60: 1528–1537
12. Y. Kim, J. C. Lee Processing and interfacial bonding strength of 2014 Al matrix composites reinforced with oxidized SiC particles. Mater. Sci. Eng A 2006; 420: 8–12
13. M. Hanabe and P.B. Aswath Synthesis of in-situ reinforced Al composites from Al-Si-Mg-O precursors. Acta Mater. 1997; 45: 4067–76
14. D. Horvitz, I. Gotman, E.Y. Gutmanas, N. Claussen. In situ processing of dense Al_2O_3–Ti aluminide interpenetrating phase composites J Eur Ceram Soc 2002; 22: 947–54
15. Z. Yu, N. Zhao, E. Liu, C. Shi, X Du, J Wang Fabrication of aluminum matrix composites with enhanced mechanical properties reinforced by in situ generated $MgAl_2O_4$ whiskers Composites: Part A 2012; 43: 631–634
16. Y.M. Youssef, R.J. Dashwood, P.D. Lee Effect of clustering on particle pushing and solidification behaviour in TiB_2 reinforced aluminium PMMCs Composites: Part A 2005; 36: 747–763
17. V. M. Sreekumar, R. M. Pillai,w and B. C. Pai Synthesis of an Al/$MgAl_2O_4$ In situ Metal Matrix Composite from Silica Gel. J. Am. Ceram. Soc. 2007; 90 [9]: 2905–2911
18. V.M. Sreekumar, K.R. Ravi, R.M. Pillai, B.C. Pai, and M. Chakraborty Thermodynamics and Kinetics of the Formation of Al_2O_3/ $MgAl_2O_4$/MgO in Al-Silica Metal Matrix Composite. Metall. Mater. Trans. A 2008; 39A: 919-933
19. N. Eusthathopoulose Dynamics of Wetting in Reactive Metal/Ceramic Systems. Acta. Mater. 1998; 46(7): 2319–27
20. J. G. Legoux, G. L'esperance, L. Salvo, and M. Suery Proceedings of the Fabrication of Particulates Reinforced Metal Composites, ASM, Montreal, 1990 p. 31
21. D. D. Jayaseelan, S. Zhang, S. Hashimoto, W. E. Lee Template formation of magnesium aluminate ($MgAl_2O_4$) spinel microplatelets in molten salt. J Eur Ceram Soc 2007; 27: 4745–4749
22. G. I. Eskin Cavitation mechanism of ultrasonic melt degassing. Ultrason. Sonochem. 1995; 2: 137–141.
23. K.S. Suslick and G.J. Price Applications of ultrasound to material chemistry. Annu. Rev. Mater. Sci. 1999; 29: 295–326.
24. J. Yan, Z. Xu, L. Shi, X. Ma, S. Yang Ultrasonic assisted fabrication of particle reinforced bonds joining aluminum metal matrix composites. Mater Des 2011; 32: 343-347.
25. V. M. Sreekumar On the formation of Magnesium Aluminate spinels in-situ in molten Aluminium-Magnesium alloys mixed with silica particles, PhD thesis, 2008
26. M. Easton, C. Davidson, D. StJohn Proceedings of the 12th International Conference on Aluminium Alloys, September 5-9, 2010, Yokohama, Japan pp 173-178
27. Y. Yang, J. Lan, X. Li Study on bulk aluminum matrix nano-composite fabricated by ultrasonic dispersion of nano-sized SiC particles in molten aluminum alloy. Mater. Sci. Eng. A 2004; 380: 378–383.
28. B. Dutta, M.K. Surappa Directional Dendritic Solidification of a Composite Slurry: Part I. Dendrite Morphology. Met. Trans. A 1998; 29: 1319–1327

29., T.V. Atamanenko, D.G.Eskin, L.Zhang and L.Katgerman Criteria of Grain Refinement Induced by Ultrasonic Melt Treatment of Aluminum Alloys Containing Zr and Ti. Metall. Mater. Trans. A 2010; 41A: 2056-66
30. R. Schweinfest, S. Köstlmeier, F. Ernst, C. Elsäser, T. Wagner, M. W. Finnis Atomistic and electronic structure of Al/$MgAl_2O_4$ and Ag/$MgAl_2O_4$ Interfaces
Phil. Mag 2001; 81[4]: 927-955
31. Z.P. Luo Crystallography of SiC/$MgAl_2O_4$/Al interfaces in a pre-oxidized SiC reinforced SiC/Al composite. Acta Mater. 2006; 54: 47–58
32. T.E. Quested, A.L. Greer Grain refinement of Al alloys: Mechanisms determining as-cast grain size in directional solidification. Acta Materialia 2005; 53: 4643–4653
33. P.L. Zak, J. Lelito, J.S. Suchy, W.K. Krajewski, K. Haberl, and P. Schumacher Influence of SiC particles size and undercooling on AZ91 based composite heterogeneous nucleation model parameters. World J. Eng. 2011; 8 (3): 269–74
34. J.B. Ferguson, Hudo, F. Lopez, P. K. Rohatgi, Kyu Cho, Chang-Soo Kim Impact of volume fraction and size of reinforcement particles on the grain size in metal matrix and nano composites. Metall. Mater. Trans. A 2014; 45A: 4055-4061
35.V.M. Sreekumar , N. Hari Babu, D. G. Eskin, Z. Fan Grain refinement efficiency of a new oxide-containing master alloy for aluminium casting alloys. Materials Science Forum 2014; 155: 794-796
36. M. Easton and D. StJohn Grain Refinement of Aluminum Alloys: Part I. The Nucleant and Solute Paradigms—A Review of the Literature Metall.Mater.Trans.A 1999; 30A: 1613-1623
37. S. Ji, D. Watson, Y. Wang, M. White, Z. Fan Effect of Ti Addition on Mechanical Properties of High Pressure Die Cast Al-Mg-Si Alloys**.** Materials Science Forum 2013; 765: 23-27
38. L. Qian, T. Kobayashi, H. Toda, T. Goda, Z.G. Wang Fracture toughness of a 6061Al matrix composites reinforced with fine SiC particles. Mater. Trans 2002; 43[11]: 2838-2842.
39. C. S. Kim , I. Sohn, M. Nezafati , J. B. Ferguson, B. F. Schultz, Z. B. Gohari , P. K. Rohatgi, K. Cho Prediction models for the yield strength of particle-reinforced unimodal pure magnesium (Mg) metal matrix nanocomposites (MMNCs) J Mater Sci 2013; 48: 4191–4204
40. G. Neite, K. Kubota, K. Higashi, F. Hehmann. In: R. W. Cahn, P. Haasen, E. J. Kramer, editors. Mater Sci Technol, vol. 8. Germany: Wiley-VCH; 2005. p. 115–212
41. I. Kapralik Thermal Expansion of Spinels $MgCr_2O_4$, $MgAl_2O_4$ and $MgFe_2O_4$ Chem. Zvesti. 1969; 23: 665—670